*Thermochimica Acta*, 108 (1986) 65–72
Elsevier Science Publishers B.V., Amsterdam – Printed in The Netherlands


# DTA STUDY OF THE RHABDOPHANE TO MONAZITE TRANSFORMATION IN RARE EARTH (La–Dy) PHOSPHATES

R.G. JONASSON

*Chemistry Department, University of Western Ontario, London, Ontario N6A 5B8 (Canada)*

E.R. VANCE

*Atomic Energy of Canada Limited, Whiteshell Nuclear Research Establishment, Pinawa, Manitoba R0E 1L0 (Canada)*

(Received 22 April 1986)

## ABSTRACT

The irreversible rhabdophane → monazite transformations on heating rare earth (La–Dy) phosphates occurred at higher temperatures (500–900°C) than dehydration (100–400°C) and were found to be exothermic. Transformation temperatures and possibly the enthalpies increased from La to Dy. A previous assessment of a *P*222 structure for hydrated Ho and Dy phosphates appears to be explainable in terms of a mixture of xenotime, rhabdophane and monazite-structured material. A natural sample exhibited a strong negative Ce-anomaly.

## INTRODUCTION

Hydrated rare earth (RE) phosphates having the $(RE)PO_4 \cdot xH_2O$ stoichiometry with $x \leqslant 3$ adopt the rhabdophane (light RE) or xenotime (heavy RE) crystal structure [1–3]. Other RE phosphates of the same essential stoichiometry appear to have the orthorhombic *P*222 structure. A natural example is ningyoite [4], (Ca, U, RE) $PO_4 \cdot xH_2O$, and it has also been suggested [5] that some hydrated Dy and Ho phosphates have the *P*222 structure. The rhabdophane-structured materials can be dehydrated by heating at ~ 200°C [6]; transformation to the monazite structure can be accomplished by heating to 900°C [7]. The hydrated xenotime-structured RE phosphates also dehydrate at ~ 200°C, and no structure transformations occur after heating at 900°C [2]. The *P*222 structures transform either to monazite-structured material (ningyoite [4]) or to xenotime structures (hydrated Dy, Ho phosphates [2]).

As part of a general investigation of phosphate minerals in connection with the immobilization of nuclear fuel waste, some hydrated RE phosphates were examined using simultaneous thermogravimetric (TGA) and differential thermal analyses (DTA), in conjunction with X-ray diffraction (XRD).

0040-6031/86/$03.50 

EXPERIMENTAL

The hydrated RE phosphates were prepared [8] by refluxing the respective RE pyrophosphates with dilute (ca. 0.1 mol $l^{-1}$ nitric acid at selected

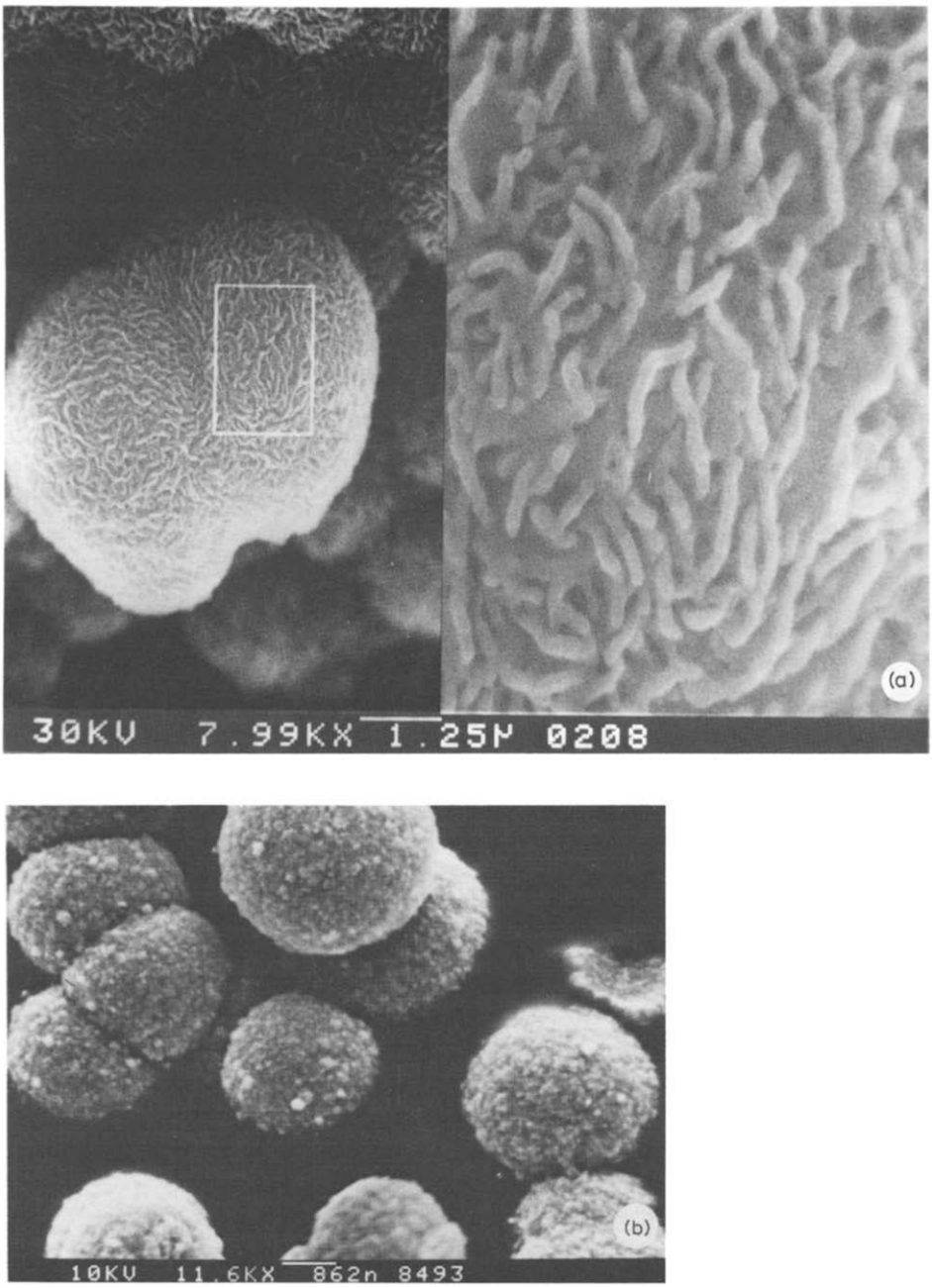


Fig. 1. Secondary electron micrographs obtained from various hydrous RE phosphates. (a) RE = La (the bar scale refers to the left-hand photograph); (b) RE = Yb.

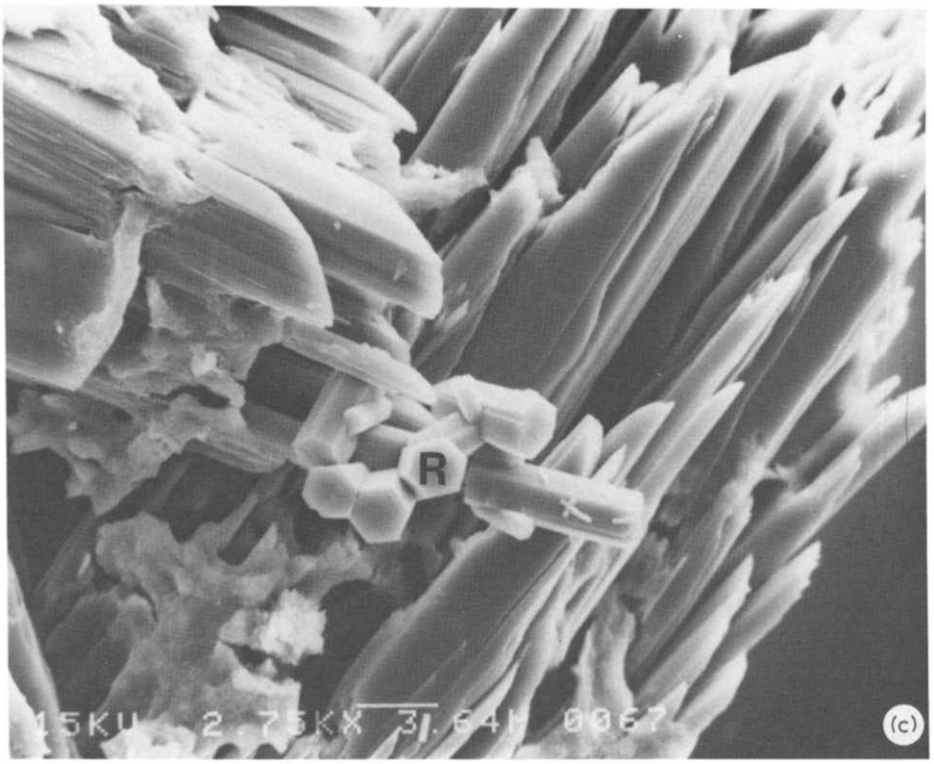


Fig. 1 (c) RE = Dy, note hexagonal rhabdophane-structured material (denoted by R) in the central region, surrounded by xenotime-structured crystals.

temperatures at or below 100°C. Needle-like crystals, ~ 1 $\mu$m in width and several micrometres long, were thus obtained for some of the materials, while in other cases ~ 3-$\mu$m sized, near-spherical aggregates of very fine crystallites were formed (Fig. 1). The samples were isolated using 0.45-$\mu$m Millipore filters, washed with distilled water and dried at 80°C for 2 h. A sample of natural rhabdophane from the Smithsonian Institution, Washington, DC (location; Idaho, U.S.A.; sample number: 121789) was also studied.

Simultaneous differential thermal anaysis (DTA) and thermogravimetric analysis (TGA) measurements were made at temperatures up to 1300°C with a Stanton-Redcroft STA-781 instrument using a heating rate of 10°C $min^{-1}$, 50–100 mg of sample, $\alpha$-$Al_2O_3$ as an inert reference, and an atmosphere of flowing air or argon. X-ray powder diffraction patterns were subsequently obtained with a diffractometer fitted with a graphite monochromator, using Cu $K_\alpha$ radiation. Powder infrared (IR) spectra were obtained over the 400–4000 $cm^{-1}$ range on a Nicolet MX-1 instrument using 0.5–3 mg of finely divided sample mixed with 300 mg of KBr to make a 12.7-mm diameter pellet. Secondary ion mass spectra (SIMS) were obtained on a Cameca IMS 3f instrument operating in the "specimen-isolation"

mode [9,10]. Powders were mounted on copper tape, and electrically isolated from the sample holder; the copper tape was also analysed to correct for interferences.

## RESULTS AND DISCUSSION

### *Synthetic samples*

Infrared spectra of the materials agreed well, in general, with previous results [2], but it was not easy to decide whether or not shoulders were present on certain of the absorption peaks. The DTA/TGA results are summarized in Table 1. Also shown are transformation temperatures, $T_x$, obtained by heating samples in an electric furnace for 1 h at temperatures 100°C apart between 400 and 1000°C. Two DTA curves are shown in Fig. 2(a): one for $GdPO_4 \cdot xH_2O$ showing a strong exothermic peak at 815 ± 5°C, and one for $LaPO_4 \cdot xH_2O$ yielding no such peak. XRD showed that a sample of hydrated $GdPO_4$ heated in the DTA/TGA apparatus to 780°C, just below the DTA peak temperature, and then quickly cooled to room temperature by switching off the heater, had the rhabdophane structure, while another sample heated to 830°C and similarly cooled had the monazite structure. Thus the exothermic peak corresponded to the structure transformation, which was irreversible.

Like $LaPO_4 \cdot xH_2O$, the hydrated Ce, Pr and Nd phosphates yielded weak or unobservable exothermic peaks, while the Sm phosphate, like $GdPO_4 \cdot xH_2O$, showed a strong peak, suggesting that the heat of transformation increases with atomic number, until those REs that form xenotime-structured hydrated phosphates are reached. The transformation temperatures (see Fig. 3) increased with increasing atomic number. The low-temperature endothermic peaks shown in Fig. 2(a) are associated with loss of water of crystallization, as shown by the TGA results in Fig. 2(b).

We now discuss the $DyPO_4$ structure. The angular positions of the XRD lines for our hydrated $DyPO_4$ agreed well with those of Donaldson et al. [5], but unlike the previous results [5], the lines having $\sin^2\theta$ values of 0.02853, 0.04965 and 0.08930 were strong compared with the others in the present work, and some "extra" lines were observed at higher values of $\sin^2\theta$ ($> 0.1$). Moreover, the angular misfit of the lowest-angle line having $\sin^2\theta = 0.02853$ with that predicted for the orthorhombic $P222$ structure [5] is nearly 0.6° in $2\theta$.

An alternative to the $P222$ assignment [5] is a mixture, principally Dy-xenotime plus Dy-rhabdophane. In this interpretation, the very weak line at $\sin^2\theta = 0.06558$ corresponds to the strongest line in the monazite pattern (the remaining monazite lines, therefore, being too weak to observe),

TABLE 1

Results of DTA/TGA (10°C $min^{-1}$) and isochronal (1 h) heating for hydrated phosphates, $REPO_4 \cdot xH_2O$

| RE | $T_p$ (°C) | Initial phase | $T_w$ (°C) (±5°C) | $x$ | $T_c$ (°C) (±10°C) | $T_x$ (°C) (±50°C) | Final phase (> 900°C) |
|---|---|---|---|---|---|---|---|
| La | 100 | M | 100, 230 | 0.7 | (a) | – | M |
| | 25 | R | 100, 230 | 1.6 | (a) | 500 | M |
| Ce | 100 | M+R | 80, 200 | 0.6 | 700 (w) | 600 | M |
| | 60 | R | 100, 250 | 1.0 | 715 (vw) | 600 | M |
| Pr | 100 | R | 120, 250 | 0.7 | (a) | 700 | M |
| Nd | 100 | R | 100, 230 | 0.7 | 790 (vw) | 700 | M |
| | 100 | R | 110, 230 | 0.7 | 680 (vw) | 700 | M |
| Sm | 100 | R | 80, 220 | 1.0 | 800 (m) | 700 | M |
| Gd | 100 | R | 210 | 0.8 | 815 (s) | 800 | M |
| Dy | 60 | X+R | 80, 180 | 1.0 | 950 (w) | 900 | X * |
| Ho | 100 | X | 110 | 1.4 | – | – | X |
| Er | 100 | X | 110 | 0.8 | – | – | X |
| Yb | 100 | X | 65 | 1.1 | – | – | X |
| Mixed (natural) | ? | R+M | 120, 230 | 1.7 | (a) | (b) | M |

$T_p$ = preparation temperature, $T_w$ = endothermic peak temperature(s), $T_c$ = exothermic peak temperature, $T_x$ = structure transformation temperature derived from isochronal heating experiments; R = rhabdophane, M = monazite, X = xenotime; $x$ deduced from weight-loss results; s = strong, m = medium, w = weak, vw = very weak; (a) = absent, (b) = insufficient sample available to carry out measurements.

* R → M → X transformations occurred at $T > 900$°C.

Underlining denotes dominant phase or stronger endothermic peak.

while the three above-mentioned lines correspond to the stronger peaks in the xenotime pattern; the "extra" lines are due to weaker lines in the xenotime pattern and the remaining lines are from the rhabdophane structure.

After our $DyPO_4$ sample was heated in the DTA/TGA apparatus at 10°C $min^{-1}$ to 950°C (the temperature of the exothermic peak) and quickly cooled, the XRD lines here attributed to the rhabdophane structure disappeared and a monazite pattern in which the strongest line was at $\sin^2\theta = 0.06558$ (see above), became apparent. The xenotime XRD pattern remained unaltered, except for a slight sharpening of the lines. No further changes in the XRD pattern were observed in similarly heating the sample to 1000°C and cooling, but heating to 1050°C, followed by rapid cooling, caused

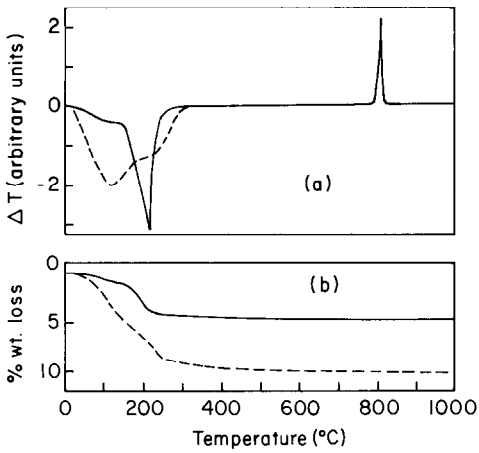


Fig. 2. (a) DTA curves (heating rate 10°C $min^{-1}$) for hydrated $GdPO_4$ (solid line) and $LaPO_4$ (dashed line). (b) Associated TGA curves.

complete conversion to the xenotime structure. No exothermic or endothermic DTA peaks were observed between 950 and 1050°C, or at higher temperatures.

*Natural rhabdophane*

The XRD pattern of the natural sample corresponded to that of rhabdophane, with monazite-structured material as a minor phase (ca. 5%). A powder IR spectrum of the material agreed well with those obtained for synthetic La and Nd rhabdophanes, except that extra absorption bands, due to $OH^-$, were observed at 1400, 1460, 3625 and 3700 $cm^{-1}$. These bands were much weaker than the broad band in the 2600–3700 $cm^{-1}$ range due to water.

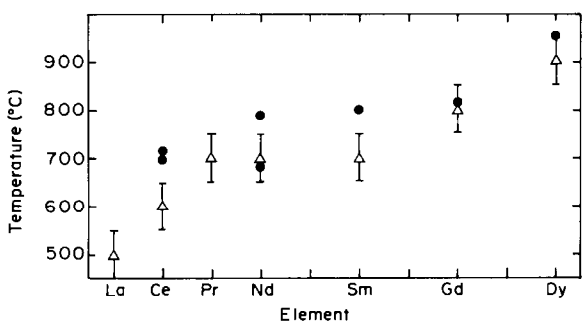


Fig. 3. Transformation temperatures as function of RE. (△) Derived from isochronal heating experiments, (●) from DTA data.

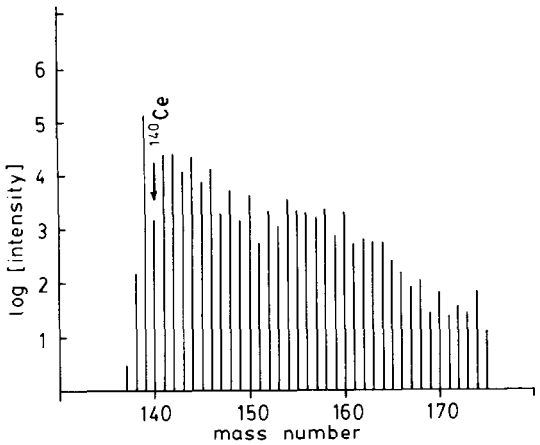


Fig. 4. RE intensities (proportional to concentrations) in SIMS experiment on natural rhabdophane.

Elemental analysis by SIMS indicated the following principal metallic elements (in addition to P) in order of decreasing abundance: La, Nd, Y, Gd, Sm and Ca. A SIMS bar graph for mass numbers in the RE region is shown in Fig. 4. (Additional details of the SIMS results are available from the authors.) The relative deficiency of Ce (compare with data of Mitchell [7] and Bowles and Morgan [6]) may be explainable if oxidizing conditions prevailed during the formation of the sample; Sawka et al. [11] also observed a negative Ce anomaly and assigned it to the same cause. In this case, Ce would be present mainly as $Ce^{4+}$ and it is possible that, as found for monazite [12], $Ce^{4+}$ cannot be readily incorporated in the rhabdophane structure, even when charge compensators such as $Ca^{2+}$ are present. Alternatively, $Ce^{4+}$ may have precipitated out of the precursor rhabdophane growth solution, before rhabdophane itself crystallized.

DTA/TGA runs were carried out in flowing air and flowing argon (the latter to prevent an exothermic peak due to oxidation of any organic contaminant). The results were very similar. No exothermic peaks due to crystallographic transformation were observed, though XRD showed that transformation to the monazite structure had occurred after heating to 900°C in the DTA/TGA apparatus. The lack of an exothermic peak was consistent with the composition being rich in light RE, on the basis of the results obtained on the synthetic materials. An 11% weight decrease due to water loss corresponded an endothermic peak in the temperature range 50–300°C (see Table 1), similar to the results on the synthetic samples and those of Bowles and Morgan [6].

## CONCLUSIONS

The irreversible rhabdophane → monazite transformations on heating RE phosphates (La–Dy) were confirmed to take place after dehydration was complete and were found to be exothermic. Transformation temperatures, and possibly the associated enthalpy, increased with increasing atomic number from La to Dy. A previous assignment [5] of the $P222$ structure to hydrated Dy and Ho phosphates appears to be incorrect. A strong negative Ce-anomaly was found for the natural rhabdophane sample.

## ACKNOWLEDGEMENTS

We wish to thank I. Muir and Surface Science Western for the SIMS analysis, R.I. Haines for the IR results, J. Snider for some of the X-ray powder patterns, and I.M. George and G. Mount for the scanning electron microscopy. We also thank the Smithsonian Institution for provision of the natural rhabdophane specimen. We thank P. Taylor, J.C. Tait and P.J. Hayward for helpful comments on the manuscript. The research was funded by Atomic Energy of Canada Limited and the National Science and Engineering Research Council (through G.M. Bancroft).

## REFERENCES

1 R.C.L. Mooney, J. Chem. Phys., 16 (1948) 1003.
2 A. Hezel and S.D. Ross, Spectrochim. Acta, 22 (1966) 1949.
3 A. Hezel and S.D. Ross, J. Inorg. Nucl. Chem., 29 (1967) 2085.
4 T. Muto, R. Meyrowitz, A.M. Pommer and T. Murano, Am. Mineral., 44 (1959) 633.
5 J.D. Donaldson, A. Hezel and S.D. Ross, J. Inorg. Nucl. Chem., 29 (1967) 1239.
6 J.F.W. Bowles and D.J. Morgan, Mineral. Mag., 48 (1984) 146.
7 R.S. Mitchell, Am. Mineral., 50 (1965) 231.
8 R.G. Jonasson, G.M. Bancroft and H.W. Nesbitt, Geochim. Cosmochim. Acta, 49 (1985) 2133.
9 J.B. Metson, G.M. Bancroft, N.S. McIntyre and W.J. Chauvin, Surf. Interface Anal., 5 (1983) 181.
10 J.B. Metson, G.M. Bancroft, H.W. Nesbitt and R.G. Jonasson, Nature (London), 307 (1984) 347.
11 W.N. Sawka, J.F. Banfield and B.W. Chappell, Geochim. Cosmochim. Acta, 50 (1986) 171.
12 J.G. Pepin, E.R. Vance and G.J. McCarthy, Mater. Res. Bull., 16 (1981) 627.